AD-786 157

REAL-TIME CORRECTION OF ATMOSPHERI-
CALLY DEGRADED TELESCOPE IMAGES
THROUGH IMAGE SHARPENING

Richard A. Muller, et al

Stanford Research Institute

Prepared for:

Defense Advanced Research Projects Agency

July 1974

REPORT DOCUMENTATION PAGE		READ INSTRUCTIONS BEFORE COMPLETING FORM
1. REPORT NUMBER	2. GOVT ACCESSION NO	3 RECIPIENT'S CATALOG NUMBER *AD 786 157*
4. TITLE (and Subtitle) REAL-TIME CORRECTION OF ATMOSPHERICALLY DEGRADED TELESCOPE IMAGES THROUGH IMAGE SHARPENING		5. TYPE OF REPORT & PERIOO COVEREO Technical Report JSR-73-9
		6 PERFORMING ORG. REPORT NUMBER SRI Project 3000
7. AUTHOR(s) Richard A. Muller Andrew Buffington		8 CONTRACT OR GRANT NUMBER(s) Contract DAHC15-73-C-0370
9. PERFORMING ORGANIZATION NAME ANO ADORESS Stanford Research Institute Menlo Park, California 94025		10. PROGRAM ELEMENT, PROJECT, TASK AREA & WORK UNIT NUMBERS
11. CONTROLLING OFFICE NAME ANO ADORESS Defense Advanced Research Projects Agency 1400 Wilson Boulevard Arlington, Virginia 22209		12. REPORT OATE July 1974
		13. NO. OF PAGES 50
14 MONITORING AGENCY NAME & ADDRESS (if diff. from Controlling Office)		15. SECURITY CLASS. (of this report) UNCLASSIFIED
		15a. OECLASSIFICATION/DOWNGRADING SCHEOULE

16. OISTRIBUTION STATEMENT (of this report)

Approved for Public Release; Distribution Unlimited.

17. OISTRIBUTION STATEMENT (of the abstract entered in Block 20, if different from report)

18. SUPPLEMENTARY NOTES

19. KEY WOROS (Continue on reverse side if necessary and identify by block number)

Telescope	Image Restoration,	Sharpness Function
Image Sharpness	Real Time	Image Quality
Atmospheric Distortion, Correction for	Optics Compensation	Rubber Mirror
	Optical Phase Shifter	Speckle Interferometer

20. ABSTRACT (Continue on reverse side if necessary and identify by block number)

A new technique for the correction of atmospheric distortion in a telescope is presented. Most of this distortion arises from a random phase variation in the incoming light across the telescope aperture. This variation limits the resolving power of even large telescopes to about one second of arc. If one defines the "sharpness" value of the images in a suitable way, this sharpness is maximized only when the phase distortion of the incoming light is zero. The

(continued)

DD FORM 1 JAN 73 **1473**

EDITION OF 1 NOV 65 IS OBSOLETE

19. KEY WORDS (Continued)

Intensity Interferometer
Seeing, Atmospheric
Steller Interferometer
Active Optics
Real-Time Optics Adjustment

20 ABSTRACT (Continued)

report presents computer simulations of a simple feedback system in which flexible optical elements, adjusted to maximize the sharpness, correct most of the atmospheric distortion. Photon statistics set the limiting magnitude of the object for which a practical feedback system can work. One should be able to resolve details in a 7th-magnitude object to better than 0.1 second of arc. The system can be conveniently employed within existing telescopes.

ABSTRACT

A new technique for the correction of atmospheric distortion in a telescope is presented. Most of this distortion arises from a random phase variation in the incoming light across the te'escope aperture. This variation limits the resolving power of even large telescopes to about one second of arc. If one defines the "sharpness" value of the images in a suitable way, this sharpness is maximized only when the phase distortion of the incoming light is zero. The report presents computer simulations of a simple feedback system in which flexible optical elements, adjusted to maximize the sharpness, correct most of the atmospheric distortion. Photon statistics set the limiting magnitude of the object for which a practical feedback system can work. One should be able to resolve details in a 7th-magnitude object to better than 0.1 second of arc. The system can be conveniently employed within existing telescopes.

ii

PREFACE

CONTENTS

ILLUSTRATIONS

TABLE

I INTRODUCTION

The resolving power of optical astronomical telescopes with aperture greater than about 10 cm has been limited by atmospheric distortion rather than by diffraction, ever since the first astronomical telescopes were built hundreds of years ago.[1*] Except on unusually calm nights at the best observatory locations, atmospheric "seeing" limits the resolving angle of large telescopes to about 1 second of arc, the diffraction limit of a 10-cm-diameter telescope. This limit has rendered impossible the imaging of the disks of nearby stars, close binary systems, and the detailed structure of the cores of galaxies. It has also prevented the high-quality imaging of the planets that would otherwise be achievable with existing large telescopes.

Attempts to lessen atmospheric distortion by locating the observatory at high altitudes have been only partially successful. Airborne observatories have seeing limitations similar to those on mountaintops, attributed to boundary-layer turbulence close to the airplane.[2] Balloon-borne systems[3] avoid atmospheric distortion, but the difficulties associated with balloon-flight operations make this technique impractical for an extended program of astronomical measurements. Until we enter a new era of large telescopes in space, atmospheric distortion will remain a major concern of astronomers.

Michelson and Pease were the first to overcome the 1 second-of-arc limit.[4] Although their stellar interferometer was incapable of complete

---

* References are listed at the end of the report.

image restoration, it permitted the first measurements of stellar diameters, close binary star systems, and the size of Jupiter's moons. Considerable improvements on interferometer techniques have been made by Hanbury Brown and Twiss[5] and by Labeyrie and co-workers.[6] These interferometer techniques are limited by the fact that in effect they measure only the intensities of the spatial Fourier components of the object's brightness distribution. Because the relative phase information of the wave components is lost, only the auto-correlation function of the image can be constructed. Unless the object being studied has certain symmetries the image information cannot be unfolded. Multiple-optical-interferometer systems overcome this limitation,[7,8] but, because of their complexity, they have not yet been applied to astronomical objects. Code[9] has presented a review of recent progress with these techniques. In principle, if one knew the modulation transfer function of the atmosphere, one could correct the distorted image after recording it. Considerable progress has been made with this post-detection approach,[8] but because the modulation transfer function varies with position and with time, it is difficult to improve resolution by more than a factor of 2 for astronomical objects.

An alternative to post-detection processing is real-time compensation of the telescope optics system in order to cancel out the phase distortion introduced by the atmosphere. Several workers have successfully used devices to stabilize the motion of the centroid of the image.[10] Unfortunately, this technique is incapable of providing the substantial improvement necessary to yield diffraction-limited performance for all but small telescopes. Babcock[11] has suggested that an active corrector plate could be introduced into the telescope optics to compensate for the changing atmospheric phase shifts. In order to determine the amount of correction to apply to a given region of the telescope objective, Babcock suggested performing a knife-edge test on

2

each portion of the objective, using an unresolved nearby bright star as the light source. Unfortunately, this technique can work only if the light from the nearby star has experienced essentially the same atmospheric phase-shift perturbation on its path to a given place on the telescope objective as the light from the object under study. Measurements of the correlations of the distortions of resolved double stars[12,13] as well as the usual theoretical models of atmospheric disturbances[14,15] indicate that this equal perturbation begins to fail for objects being viewed by ground-based telescopes that subtend more than a few seconds of arc. The angular region for which the requirement holds is called the "isoplanatic patch." Since the atmospheric distortion changes with a time constant of about 0.02 sec,[16] application of Babcock's scheme to astronomical measurements requires that a bright unresolved star (typically 7th magnitude or brighter) lie within a few seconds of arc of the object being studied. Such nearby stars are rare. A system similar to that proposed by Babcock has been designed by Perkin-Elmer Corporation for a different problem: in situ figuring of a light-weight space telescope mirror.[17]

The technique we introduce in this report was conceived in collaboration with F. J. Dyson of the Institute for Advanced Study, Princeton. Dyson's analysis will be published separately.[18]

Our optical system requires an optical element that can shift the effective phase of the light across the aperture of the telescope. This could be accomplished either by dividing the telescope objective into separately movable segments, or, more conveniently, by introducing a movable optical element elsewhere in the system. Our technique requires no unresolved bright star nearby, for we use the light from the object under observation in order to determine the required phase shifts. In principle our technique works for an arbitrarily complex object, although the object must lie within the isoplanatic patch.

3

We now introduce the concept of image "sharpness." We can define this sharpness in such a way that under certain conditions the value of the sharpness for an atmospherically degraded image is always less than that of the true image. One such sharpness definition is

$$S_1 = \int dx dy \; I^2(x,y), \tag{1}$$

where x,y denote coordinates in the image plane, and I(x,y) is the image intensity. Figure 1 is a schematic illustration of our real-time correction scheme. We place a device capable of measurement of the image sharpness in the image plane of a telescope. The disturbing atmosphere degrades the image sharpness by randomly perturbing the phase and amplitude of the incoming light. Later in this report we show that the amplitude perturbations are unimportant for image sharpness. A phase corrector placed in the optical path is capable of restoring the proper phase. Individual segments of the phase corrector are adjusted in turn to maximize the sharpness of the image, as measured by the device placed in the image plane. If the entire telescope objective can be corrected during the period of time in which the atmospheric distortion holds constant, the resulting image will be nearly diffraction-limited.

In the remainder of this report we discuss several alternative definitions of sharpness. In the Appendix we present proofs that some of these sharpness functions reach their maximum only for a properly restored image, one from which the atmospherically introduced phase variation has been removed. We discuss various means of choosing the most practical sharpness functions. We then present computer simulations of realistic telescope systems, showing that our feedback scheme properly restores images that have been degraded by simulated atmospheric phase distortions. Finally, we present the results of

4
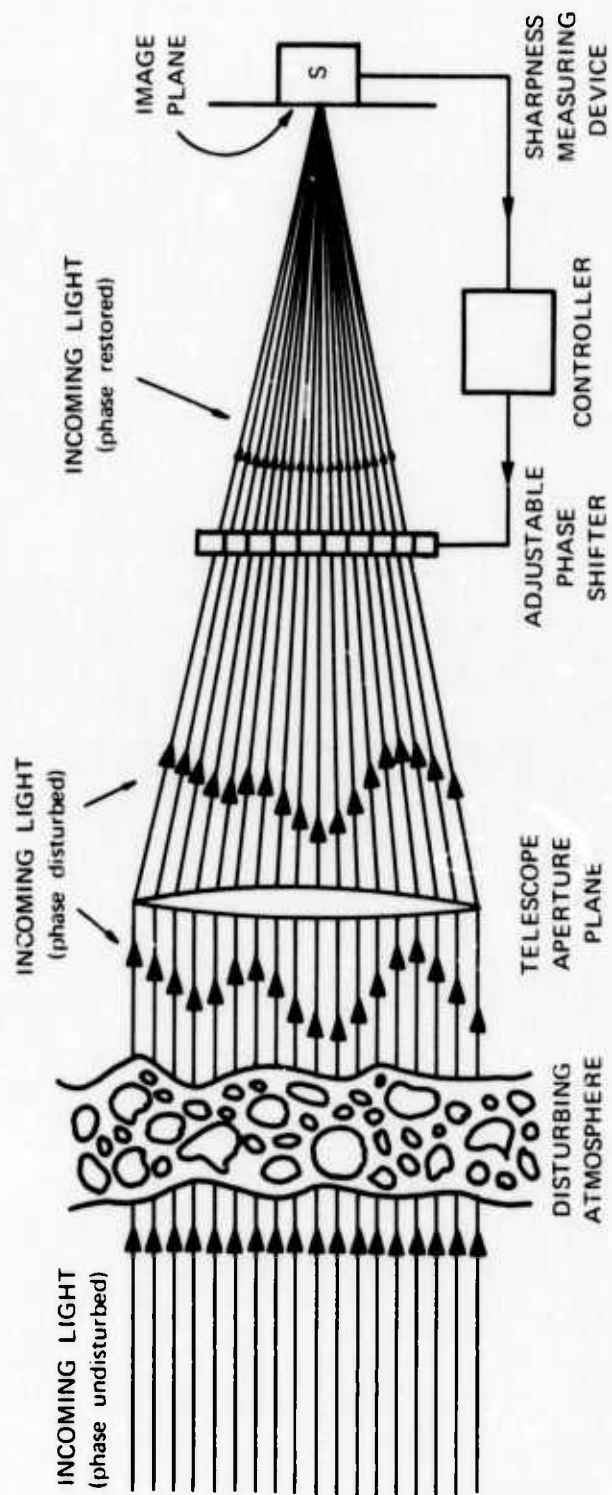
FIGURE 1   SCHEMATIC DIAGRAM OF IMAGE-RESTORING SYSTEM.   Arrowheads indicate the relative phase of the wave.   The adjustable phase-shifter (perhaps an extra flat mirror with movable segments incorporated into the optical path) corrects the phase of the incoming wave.

5

introducing statistical fluctuations into the sharpness-measuring device, showing that such fluctuations set the ultimate limitation on object brightness for which our technique produces diffraction-limited performance.

II IMAGE-PLANE SHARPNESS FUNCTIONS

A good definition of the sharpness S of an image is one for which S reaches a maximum value only for a true (undistorted) image. For the purposes of this report we consider only "aperture-plane distortion," defined below. Let $W(u,v)$ be the instantaneous wavefront at the telescope aperture in the absence of any distortion. If the distorted wavefront $W'(u,v)$ is given by

$$W'(u,v) = W(u,v) \cdot \Delta(u,v) \tag{2}$$

then we have aperture-plane distortion. Here $\Delta(u,v)$ is any complex function of the position (u,v) in the plane of the aperture. Spherical aberration can be expressed in this way and is therefore an example of aperture plane distortion. Under certain conditions, atmospheric distortion can also be expressed by this formula. If the object being viewed by a ground-based telescope is of sufficiently small angular extent that light from all parts of the object incident on the same point (u,v) has passed through essentially the same perturbing atmosphere, then we have aperture-plane distortion. Such an object is said to lie within a single "isoplanatic patch."

The flexible optical element of Figure 1 allows us to add extra phase-shifts to the $\Delta(u,v)$, in hopes of reducing or eliminating the distortion. We want to define the sharpness S in such a way that any $\Delta(u,v)$ (which now includes the effects of correction as well as the original distortion) other than a simple translation of the image $\left[\Delta(u,v) = e^{ik(a+bu+cv)}, \text{ where a, b, and c are constants}\right]$ will reduce the value of S.

Table 1

SATISFACTORY DEFINITIONS OF IMAGE-PLANE SHARPNESS[*]

Definition	Computer Simulation	Comments[+]
$S_1 = \int dx\, dy\, I^2$	Satisfactory	Proven (see Appendix).
$S_2 = I(x_o, y_o)$	Satisfactory	Makes poor use of photon-counting statistics, so satisfactory only for bright objects.
$S_3 = \int dx\, dy\, MI$	Satisfactory for M = round hole, I = single or multiple stars	Proven if $M = I_o$ = undistorted image. Reduces to S_2 if $M = \delta(x_o, y_o)$.
$S_4 = \int dx\, dy \left\| \dfrac{\partial^{m+n} I(x,y)}{\partial x^m \partial y^n} \right\|^2$	Untried	Proven.
$S_5 = \int dx\, dy\, I^n$ $\quad n \geq 2$	Satisfactory for $n = 2, 3, 4$	Proven only for unresolved star.
$S_6 = -\int dx\, dy\, I\, r^2$ $\quad r^2 = x^2 + y^2$	Poor	Moment of inertia function. Proven. Reduces tails of light distribution but gives poor central maximum. A special case of S_3.
$S_7 = -\int dx\, dy\, \ln(I!)$ $\quad \simeq -\int dx\, dy\, I \ln(I)$	Satisfactory	Minimizes the "entropy" of the image. Quantization of I (photons) gives meaning to $I!$
$S_8 = -\int dx\, dy\, \|I - I_o\|^n$	Untried	"Defect function." Proven.

[*]In preparing this report for publication we found that at least S_1, S_3, and S_6 have appeared before in the optics literature, although we had not seen them when we did this work. See, for example, E. H. Linfoot.[19]

[+]Many of the proofs are due, in whole or in part, to Freeman Dyson.

8

There are many definitions of image sharpness S which satisfy this criterion. An example (mentioned in the introduction) is $S_1 = \int dx\, dy\, I^2(x,y)$, where $I(x,y)$ is the intensity at a point (x,y) in the image plane of the telescope system. In the Appendix we prove that for monochromatic light, S_1 reaches its maximum value only when $A(u,v)$ is reduced to no more than the image translation described above. The proof is done by using a version of the Fresnel-Kirchoff equation to calculate the intensity. S_1 is maximized for zero distortion irrespective of the object intensity distribution. We can therefore use S_1 to provide feedback to the active optical elements and remove the distortion, even for complex objects such as planets and galactic cores (if they lie within an isoplanatic patch). There is no way that aperture distortion can increase the value of S_1 beyond its undistorted value even for an arbitrarily complex object.

The second law of thermodynamics suggests another definition of sharpness. Let $S_2 = I(x_0, y_0)$, the brightness of the image at an arbitrary point (x_0, y_0) on the image plane. For objects that have a brightest spot, we believe S_2 will be maximized when the image of that bright spot is shifted over to the point (x_0, y_0) and also the distortion is eliminated. We have not obtained an analytic proof.

Yet a third definition of sharpness is conceptually similar to the above two definitions. Let $S_3 = \int dx\, dy\, M(x,y) \cdot I(x,y)$, where $M(x,y)$ is the transmittance of a mask placed over the image. In the case in which M is an accurate replica of the true undistorted image, S_3 is a good definition of sharpness that reduces to S_1 above when the distortion is eliminated. In the case in which M is a delta function at (x_0, y_0), S_3 reduces to S_2 above. We are investigating how closely $M(x,y)$ must match the restored image in order for S_3 to be a good definition of sharpness, and what sort of final images may result when the match is poor.

9

We have investigated several other definitions of S. In Table 1 we list the ones we believe to be good definitions of image sharpness in the sense that they reach a maximum when image distortion (excluding a simple translation) has been removed. We also indicate which functions have been tested in our computer simulations (to be described in Section IV), and which functions have a formal proof in the Appendix.

III REAL-TIME CORRECTION OF TELESCOPE OPTICS

In the previous section we introduced the concept of image sharp-
ness S, where S reaches a maximum value only when the aperture-plane
distortion has been eliminated. In this section we describe a feedback
scheme in which small optical-path-length perturbations are introduced
in the optical path as in Figure 1. The effect of these perturbations
on S is detected, and the appropriate compensation to maximize S is
determined and then permanently introduced in the optical path.

For the case of astronomical seeing, we can make several
simplifications. The distortion function $\Delta(u,v)$ typically has a
coherence length of 10 cm, corresponding to the 1 arc sec mentioned
previously. We plan to use discrete compensating segments, each one
of which affects approximately 10 cm of the incoming wave. Therefore
a telescope of aperture area A cm^2 must have approximately $A/100$
compensating elements. Of course the incident wave's distortion
function is continuous in (u,v) so the use of discrete compensating
segments leads to a residual error in the correction. In the next
section, however, we show that this residual error is small.

Another simplification results because "random apodization" of an
aperture has little distorting effect on an image. This allows us to
write $\Delta(u,v) = e^{ik\delta(u,v)}$ where $\delta(u,v)$ is purely real. In the next
section, by using computer simulation we show that ignoring amplitude
changes in the incident wave due to the disturbing atmosphere causes
little image distortion. It is not difficult to see why this is so:
the central maximum of the image of a point object has all of the
amplitudes adding up in phase, whereas at the first minimum these

11

amplitudes all cancel. A random variation of amplitudes at the telescope aperture somewhat diminishes the intensity at the central maximum, corresponding roughly to the fraction of the aperture that has been blacked out. The first minimum also gains some intensity, but for a telescope whose aperture contains many 10-cm "cells" the gain in intensity is small compared with the remaining central maximum. On the other hand, a random phase variation across the aperture completely destroys the central maximum. In fact, the average intensity expected at the original site of the first minimum and the original site of the central maximum are now approximately the same.

We plan, then, to use a compensating system that alters only the phase of the incoming wave and not the amplitude. The adjustable element could be an eidophor system as proposed by Babcock,[11] a set of movable mirror segments driven by piezoelectric or magnetostrictive transducers, or a plate of variable optical thickness (such as PLZT ceramic materials[20]).

We must correct the telescope objective within a time less than the characteristic time τ in which the atmospheric distortions change. Measurements of the frequency spectrum of stellar scintillations and of stellar speckle patterns[16] indicate that, at a good telescope site, we should have about $\tau = 0.02$ sec to make our corrections. τ for a high-altitude aircraft should be about ten times shorter. Statistical fluctuations in the number of photons arriving within the time period set the minimum photon flux of an object whose image can be corrected by this technique. Unless we have at least one detected photon for each aperture segment in the time τ, there is no possibility of making a correction. (For $\tau = 0.02$ sec, and 100 cm^2 aperture segments, this argument implies that the object under observation must be 15th magnitude or brighter). For a real system, considerably more than one photon per segment per τ is required. We will now make an order-of-

magnitude estimate for the minimum flux of the object under observation required for a real correction system to work.

Consider that n settings of an individual correction segment are necessary to determine the proper setting of that segment to maximize S. If the area of the telescope is A, and the effective area of an individual correction segment is a, then the number of individual segments is $N = A/a$. If n settings are required to position an individual segment (n = 2, typically), the time available for each setting is

$$t = \tau/nN = \tau a/nA \quad . \tag{3}$$

Let the flux of the object under observation be B, measured in terms of photons/cm^2 sec) at the aperture. Then the number p of detected photoelectrons in time t is

$$p = \eta BAt = \eta Ba\tau/n \tag{4}$$

where η is the photon detection efficiency. Statistical fluctuations dp in p are typically $\sim \sqrt{p}$. Our computer simulations show that the fractional change in a sharpness value caused by varying one segment is approximately 1/N, although a poor choice of the sharpness function can cause it to be less than this. In order to make a statistically significant measurement of the effect of the variation we must have

$$1/N \geqslant dp/p = 1/\sqrt{\eta Ba\tau/n} \quad . \tag{5}$$

Substituting $N = A/a$ we find that

$$B \geqslant nA^2 / a^3 \eta\tau \quad . \tag{6}$$

We can combine Eqs. (4) and (6) to get, simply,

$$p \geqslant N^2 \quad . \tag{7}$$

13

In the next section we verify this formula empirically with computer simulations. For $A = 10^4 cm^2$, $a = 10^2 cm^2$, $\eta = 0.25$, $n = 2$, and $\tau = 0.02$ sec, we find $B \geq 4 \times 10^4$ photons/cm^2 sec. Since the relationship between astronomical magnitude m and B (for a 0.3 μm bandpass) is*

$$B = (4 \times 10^6) \times 10^{-m/2.5} ,\qquad (8)$$

this corresponds to objects brighter than about 5th magnitude. This is, of course, only a rough estimate. By arranging the telescope geometry in the form of an annulus, one could achieve an angular resolution of about 0.02 arc sec for this example (see Section V.).

---

*Can be calculated from the quantities given by C. W. Allen.[21]

14

IV COMPUTER SIMULATIONS

We have simulated telescope systems with active feedback, using the Fresnel-Kirchoff equation in a numerical calculation of the image intensity distribution $I(x,y)$ for monochromatic light. In the cases where we formed images of complex objects, we assumed that the object flux distribution $I(\theta,\varphi)$ was spatially incoherent. To simulate the atmospheric distortion we introduced a random-walk phase variation into the incident wavefront at the telescope aperture. The characteristic distance in which this phase variation had become randomized was set to be 10 cm. Essentially identical results were given by an alternative simulation of the distortion, in which the incoming wave was divided into 10-cm portions each of whose phase was randomly varied between $\pm\pi$ radians.

To provide the simulation of actual telescope feedback systems we considered the aperture of the telescope to be broken up into N separately movable segments. We introduced a small phase shift in the portion of the incident wavefront corresponding to a single segment and calculated the changed value of the sharpness function resulting from the perturbation. The measurement of sharpness change was used to drive the feedback system, determining and setting a permanent phase correction for that particular aperture segment.

We used two feedback schemes. In the first we introduced one and then a second phase addition to the particular segment, in order to get sharpness values corresponding to perturbations of $+\pi/2$ and then $-\pi/2$ radians. Letting $S(0)$ be the original sharpness value, and $S(+)$, and $S(-)$ be the calculated sharpness values for the shifted segment phase

15

positions, we then determined the best setting for that segment, phase shift φ, using

$$\tan \varphi = [S(+) - S(-)]/[S(+) + S(-) - 2S(0)] . \qquad (9)$$

Equation (9) follows from the fact that all the sharpness functions we investigated vary nearly sinusoidally as the phase shift of any particular segment varies over its range of 2π radians.

We also used a feedback scheme that followed the gradient of the sharpness function. This scheme has the advantage of being extremely simple to build into a practical telescope system. We introduced a small perturbation of φ_o radians into an individual segment. If the sharpness value increased we left the perturbation in, and moved on to the next segment. If the sharpness value decreased, we removed the perturbation, placing the segment at $-\varphi_o$ instead, before moving onto the next segment. Although this feedback scheme did not provide the accurate segment setting of Eq. (9), it did perform nearly as well (for $\varphi_o = \pi/4$) when allowed to cycle through the N mirrors twice. However, most of the calculations we shall report in this section used the technique of Eq. (9).

We chose N = 25 aperture segments in order to simulate a relatively small telescope and yet be able to achieve a resolution significantly better than 1 arc sec. We considered two telescope geometries. The first was a strip or "flatland" mirror that we took to be 250 cm long by 10 cm wide. The images formed by such a mirror have much better resolution along the direction of the strip, so we suppressed the other dimension, presenting our calculations in just a one-dimensional image "plane." The second geometry was a ring mirror with an outer diameter of 75 cm and an inner diameter of 55 cm. For this telescope, we calculated and displayed two-dimensional images.

16

We first used our computer program to confirm our claim that phase variations in the atmospheric disturbance are much more disruptive to the image than are amplitude variations. Figure 2 shows the images with the strip mirror of a single unresolved star for (1) no atmospheric disturbance, (2) random amplitude variations in the incident wavefront, and (3) random phase variations in the incident wavefront. It is clear from Figure 2 that the amplitude variations merely reduce the height of the central maximum, while the phase variations completely disrupt the central maximum, giving a speckle pattern similar to those reported in real observations by Labeyrie.[6] In this pattern, the size of the over-all image corresponds to the seeing limit (1 arc sec), whereas the average size of individual speckles is close to the diffraction limit of the telescope.

An "iteration" of segment settings consists of a single pass through the N segments, setting each individual phase according to Eq. (9). Figure 3 shows how the atmospherically perturbed image of an unresolved star in the strip telescope improved as each of the 25 segments was adjusted in turn. The sharpness function chosen for this particular calculation was S_1 from Table 1. An image that is essentially diffraction-limited resulted after only a single iteration. In the restored image approximately half of the original flux is still spread around in residual speckles whose brightness is typically 10% that of the newly formed central maximum. The central maximum formed at the location of the brightest original speckle when sharpness functions S_1, S_5, or S_7 were used, but, as expected, it formed at the origin or (x_o, y_o) when we used function S_2, S_3, or S_6. Systems employing the latter functions use the phase-shifter array to compensate telescope tracking error as well as the atmospheric perturbations. Of course, telescope tracking can also be easily accomplished with a separate feed-back system. Figure 4 shows the original speckle pattern and restored image for the ring mirror geometry and sharpness function S_3 using for
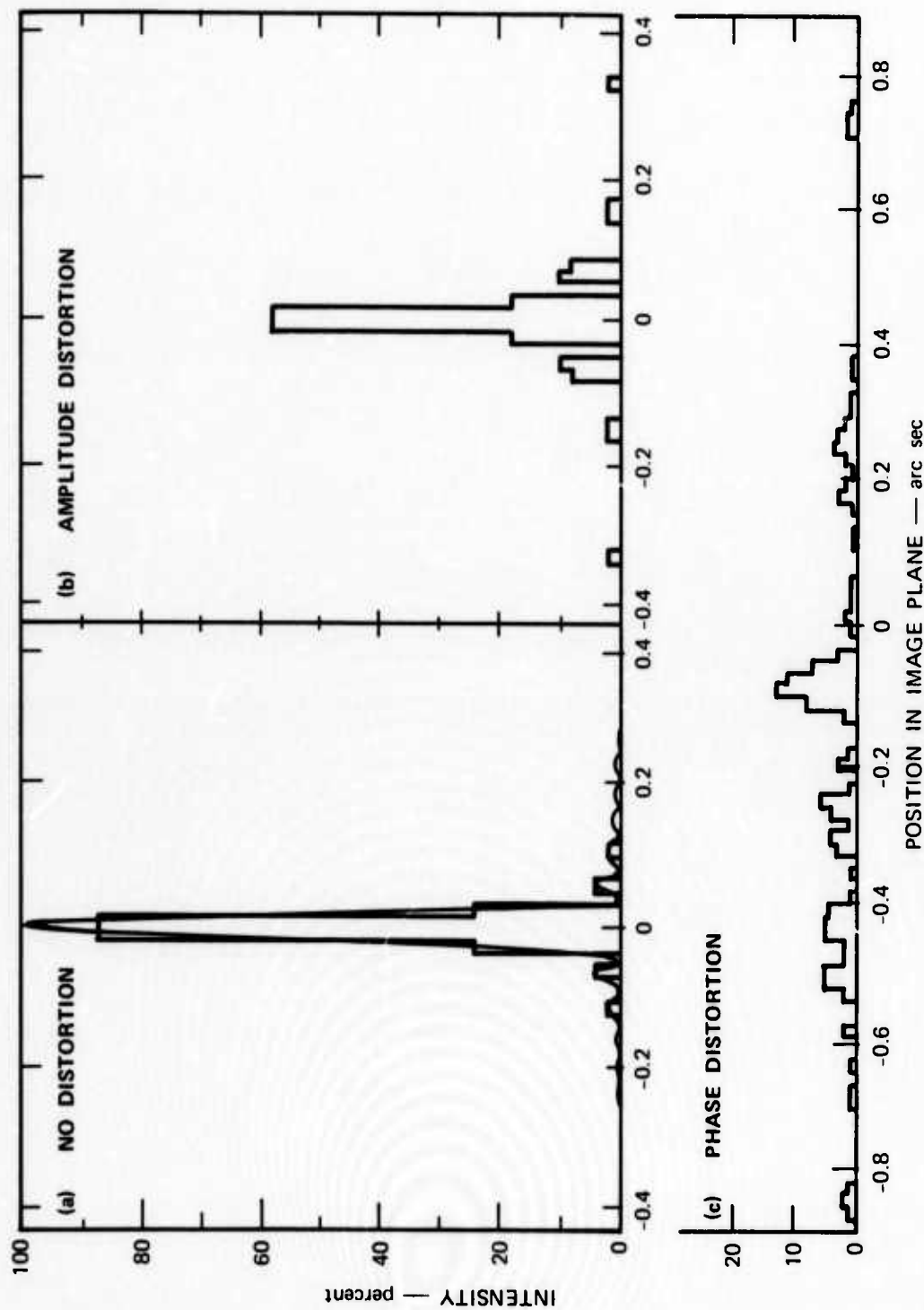
17

FIGURE 2 COMPUTER-SIMULATED DIFFRACTION PATTERNS.   (a) No disturbing atmosphere.
(b) Random amplitude variation.   (c) Random phase variation.   The telescope geometry for
this figure was a 2.5-m-long strip.   All the displays in this report are normalized so that
100% intensity is the peak for an undisturbed diffraction pattern.   The smooth curve in
(a) is a [sin(x)/x]2 diffraction pattern shape, while the histograms indicate the results of
our discrete computer calculations.

18

ONE ITERATION OF A
25 SEGMENT STRIP MIRROR
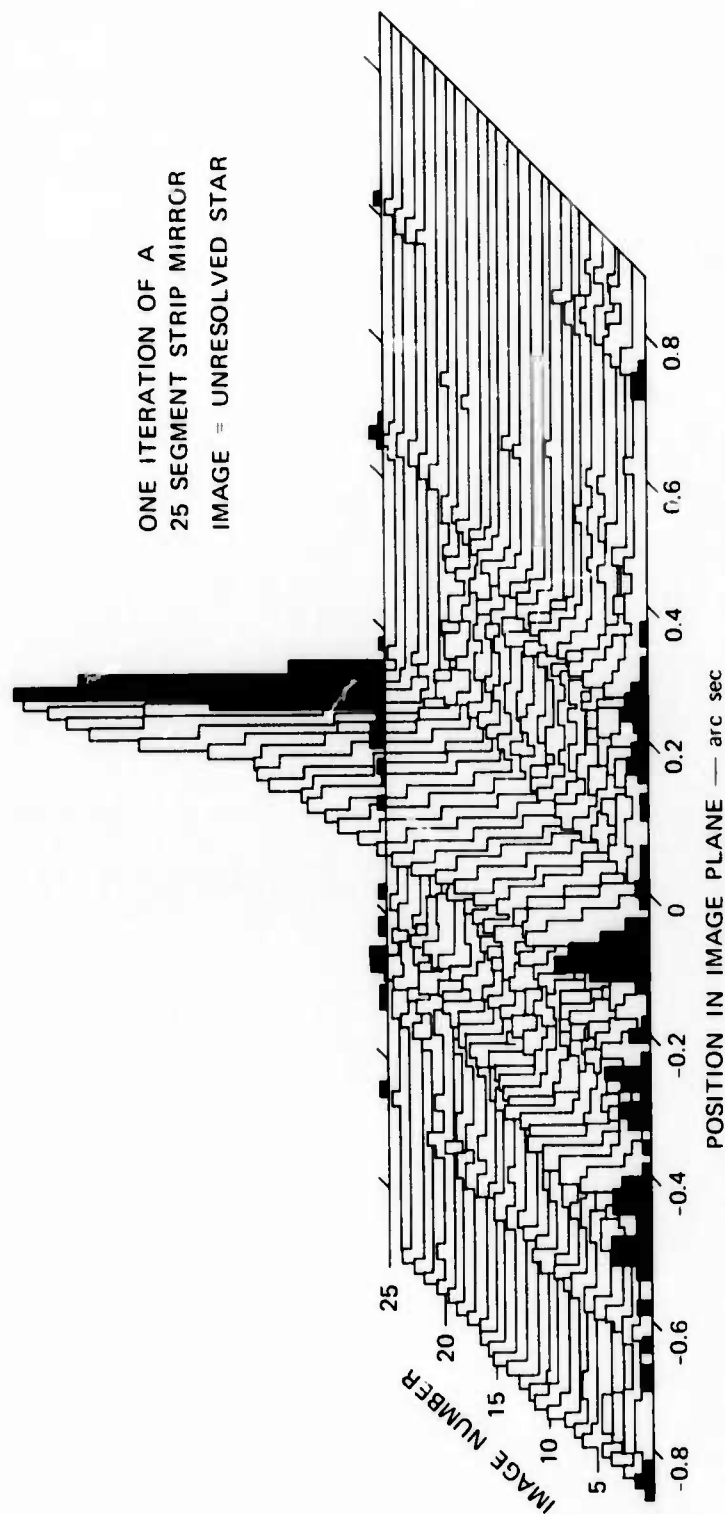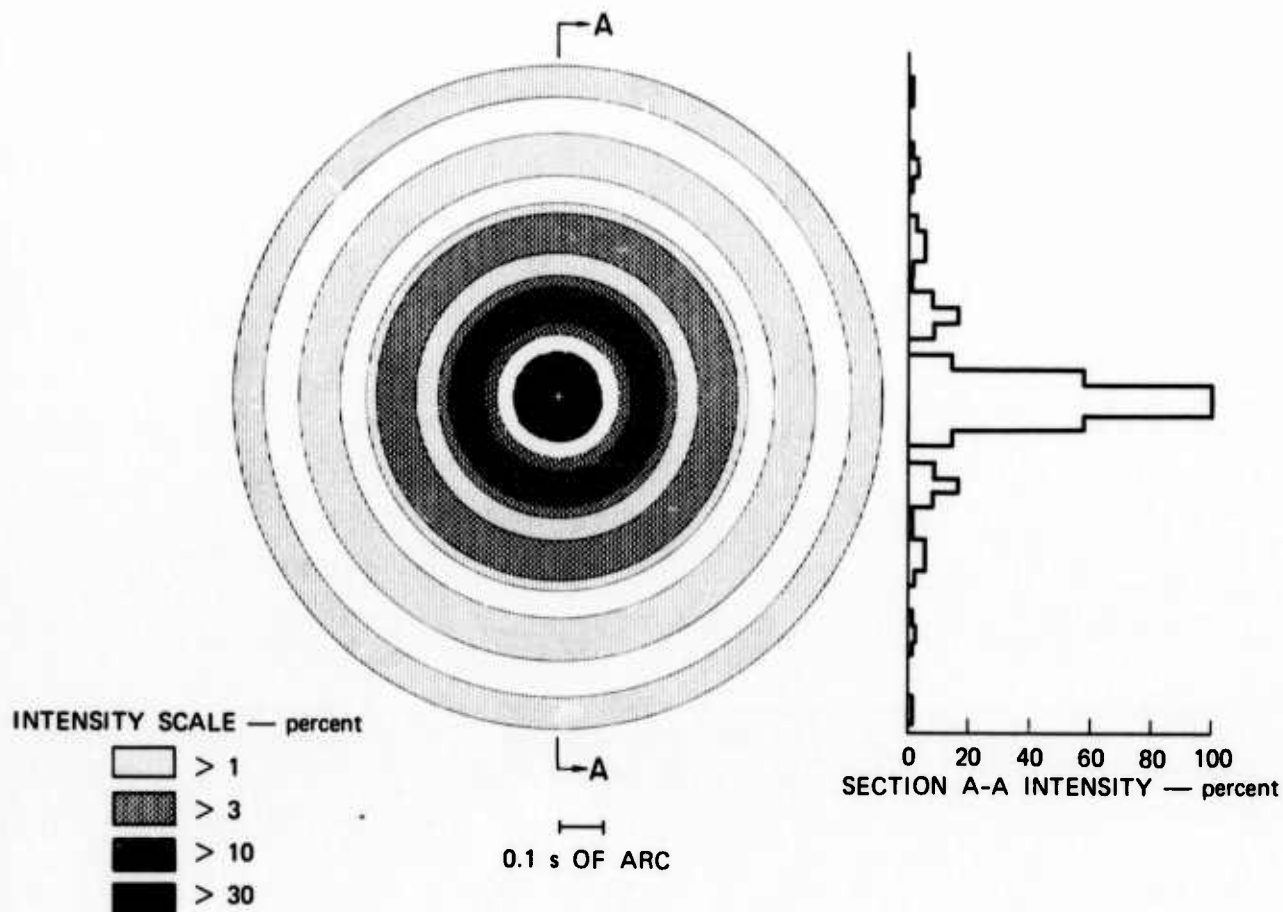IMAGE = UNRESOLVED STAR

FIGURE 3   IMAGE OF A POINT STAR AS EACH PHASE SHIFTER SEGMENT IS ADJUSTED IN
SEQUENCE. The initial image (shaded) is the same as the speckle pattern shown in
Figure 2(c). The image improves as each of the 25 segments is adjusted in turn to
compensate for the atmospheric distortion. The final diffraction-limited image (Image 25
in the figure) is also shaded. This final image formed at the position of what was
originally the brightest speckle. The sharpness function used to correct the image was
$S_1 = \int I^2$.

19

INTENSITY SCALE — percent

☐ > 1
▨ > 3
■ > 10
■ > 30

0.1 s OF ARC

SECTION A-A INTENSITY — percent

(a)   NO DISTURBING ATMOSPHERE

FIGURE 4   TWO-DIMENSIONAL IMAGES FROM A COMPUTER SIMULATION OF A RING-SHAPED TELESCOPE APERTURE. Sections of the contour plots are shown in the accompanying histograms. The contour plots (but not the histograms) have been smoothed to average our unphysical features due to the discrete nature of the computer calculations.

20
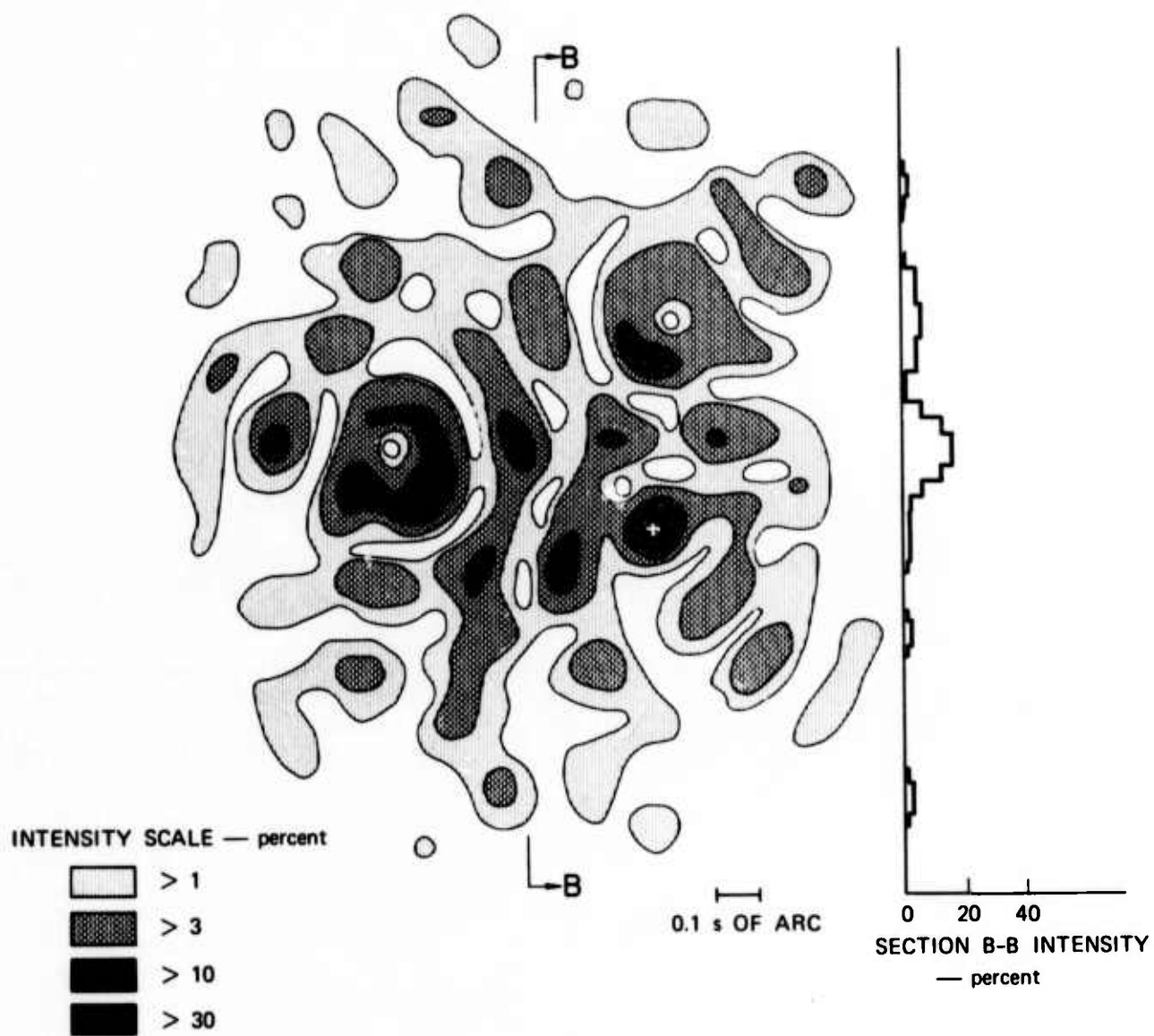
(b) SPECKLE PATTERN FOR A RANDOM PHASE DISTORTION AT THE APERTURE PLANE

FIGURE 4 (Continued)

21

INTENSITY SCALE — percent

> 1

> 3

> 10

> 30

0.1 s OF ARC

SECTION C-C INTENSITY — percent
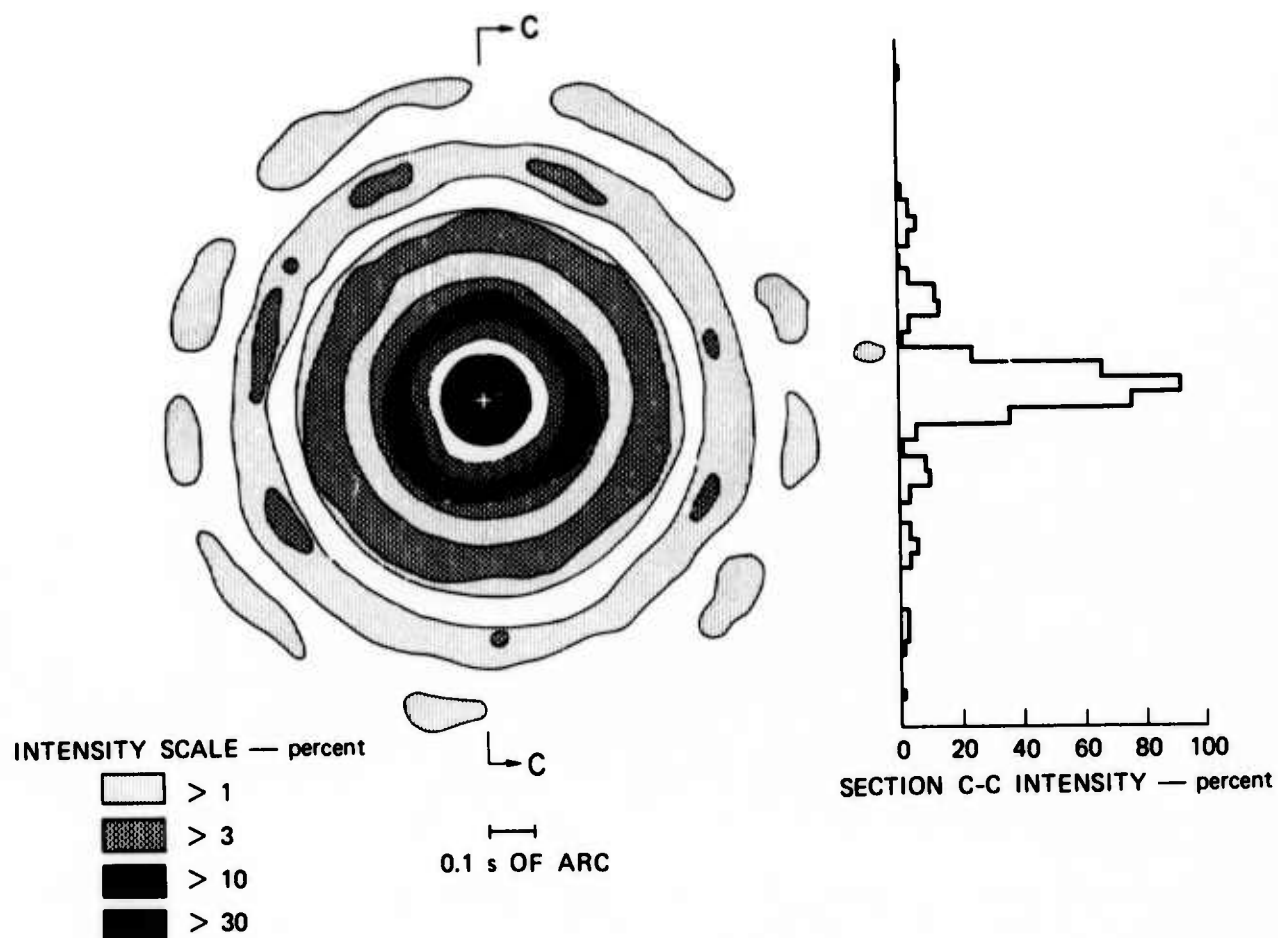
(c)   RESTORED IMAGE AFTER A SINGLE ITERATION OF THE 25 PHASE-
SHIFTER SEGMENTS, USING $S_3 = \int MI$, WITH M = A ROUND HOLE
THE SIZE OF THE CENTRAL DIFFRACTION MAXIMUM.   The ring
had an outer diameter of 75 cm and an inner diameter of 55 cm.

FIGURE 4   (Concluded)

22

the mask M a hole the size of the restored diffraction central maximum. The improvement in the image after only a single iteration is dramatic. Finally, Figure 5 shows the original speckle pattern and restored image for three stars of equal flux separated by angles of 0.04 and 0.20 second of arc, viewed by the strip mirror.

The residual speckles visible in the restored images of Figures 3 through 5 were not reduced further by subsequent iterations of the mirror system. Such a residue of speckles in the restored image is not unexpected, both in the simulations and in practice, since the perturbed wave varies continuously over the aperture, whereas we have applied the corrections to N discrete segments in the movable optical element. Figure 6 shows the initial phase distribution of the atmospherically disturbed light from an unresolved star at the telescope aperture, t‹ ether with the N values of φ calculated for this case according to Eq. (9). It is clear from Figure 6 that our applied correction is only approximate. Therefore perfect restoration of the proper straight wavefront is impossible with only 25 discrete elements, and our applied correction cannot completely restore the image. We allowed this mismatch in our simulations because we felt that such a discrete compensator might be easiest to build, using separately movable mirrors or transparent phase shifters. A single continuous mirror, deformed by discrete transducers, may have smaller residual speckles than indicated in Figures 3 through 5, since it exploits the continuity that must be present in any real incoming wavefront.

Most of the sharpness functions we tried from Table 1 converged on the same solution in one (or at most two) iterations. An exception, however, was $S_6 = \int r^2 I$, which weighted the far-away speckles so heavily that a central maximum could not form. Figure 7 shows the result of two iterations with S_6. Reduction of light in the "tails" of an image may
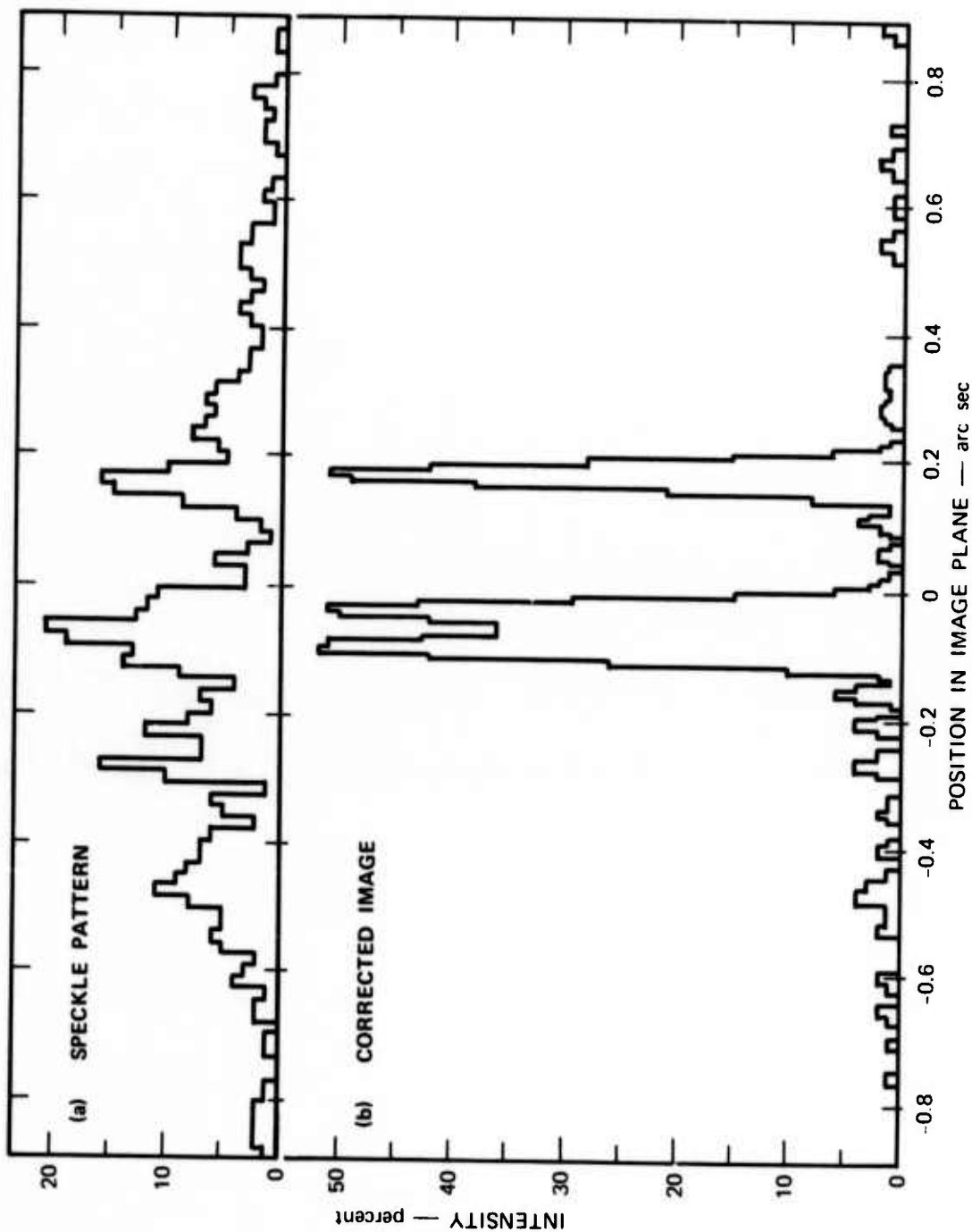
FIGURE 5   IMAGES OF A TRIPLE STAR. The 2.5-m strip telescope is used to view three stars of equal intensity and separated by 0.04 and 0.20 seconds of arc using $S_1 = \int 12$. (a) Original speckle pattern.   (b) Image after one iteration of the 25 segments.
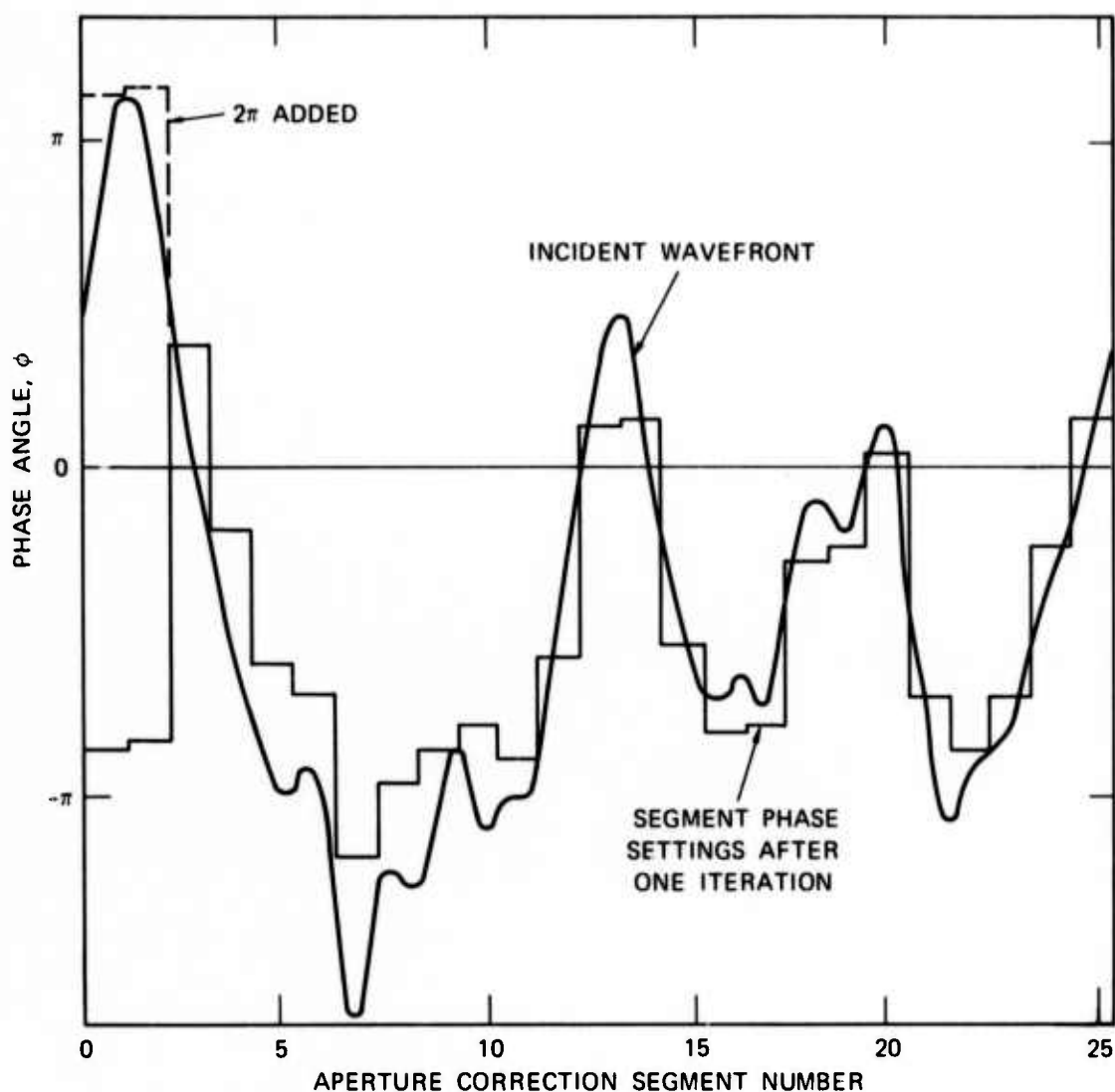
24

FIGURE 6 PHASE ANGLE vs. POSITION FOR THE RING-TELESCOPE
GEOMETRY. Position is indicated by numbering the 25
correction segments around the ring. The original disturbed
phase of the incident wave (smooth curve) and the segment
setting resulting for a single iteration (histogram) are shown.
The image resulting from this wavefront was shown in
Figure 4. Segments 1 and 2 were off by 2π and have been
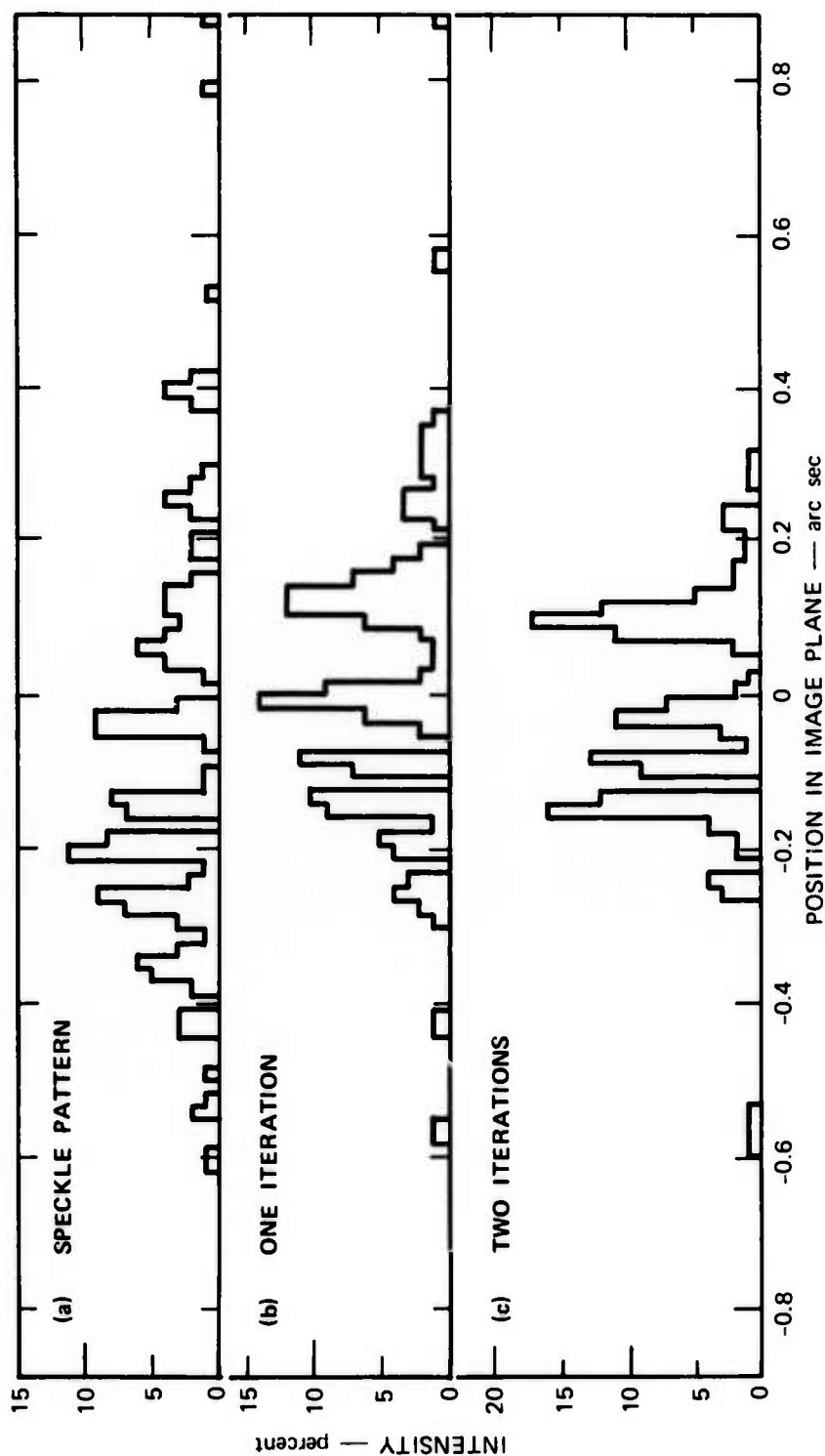redrawn (dashed) to show another equivalent position.

FIGURE 7   IMAGE OF AN UNRESOLVED STAR USING THE "MOMENT OF INERTIA" SHARPNESS FUNCTION $S_6 = \int r^2 I$. Although some improvement results, it is not comparable to that of Figure 3.   (a) Original speckle pattern.   (b) Image after one iteration of the 25 segments.   (c) After two iterations.

26

be valuable for some applications, but in most cases the central maximum formed by S_6 is too poor to be useful.

The easiest sharpness function to implement on a real telescope is S_3, since a device to make this measurement consists merely of a single photomultiplier with a mask of the desired transmittance $M(x,y)$ placed in front of it at the image plane. Our proof in the Appendix applies only in the case in which $M(x,y)$ corresponds to the true restored image $I_o(x,y)$, but we have found in the computer simulations that S_3 still works very well when M is only approximately equal to I_o. In particular, we tried an M that was a round hole in an otherwise opaque mask: the diameter of the hole was chosen to correspond to the size of the diffraction-limited image. This definition of S_3 gave results as satisfactory as those we achieved with S_1 or S_5. All sharpness functions we tried gave as good an image restoration for complex objects (double stars and triple stars) as for a single unresolved star. In practice, the choice of sharpness function depends on both ease of implementation and the type of object being observed. For objects such as binary star systems where the telescope could center on the brighter star of the pair, one would probably use the simple S_3 system. For a rapidly tumbling object such as an irregular asteroid the sharpness function S_1 might be more appropriate. For imaging the disk of a planet a function related to S_3 would probably be best, in which one maximizes the light through a narrow annular slot in the image plane.

We used our computer simulations to evaluate the effect of statistical fluctuations in the number of detected photons (photoelectrons). For each measurement of S we perturbed the number of photoelectrons in each image bin in a random way, using a Poisson distribution. Figure 8 shows the resulting image of the triple star (each star of 9th magnitude) after one iteration. For this image we used the sharpness function S_1,
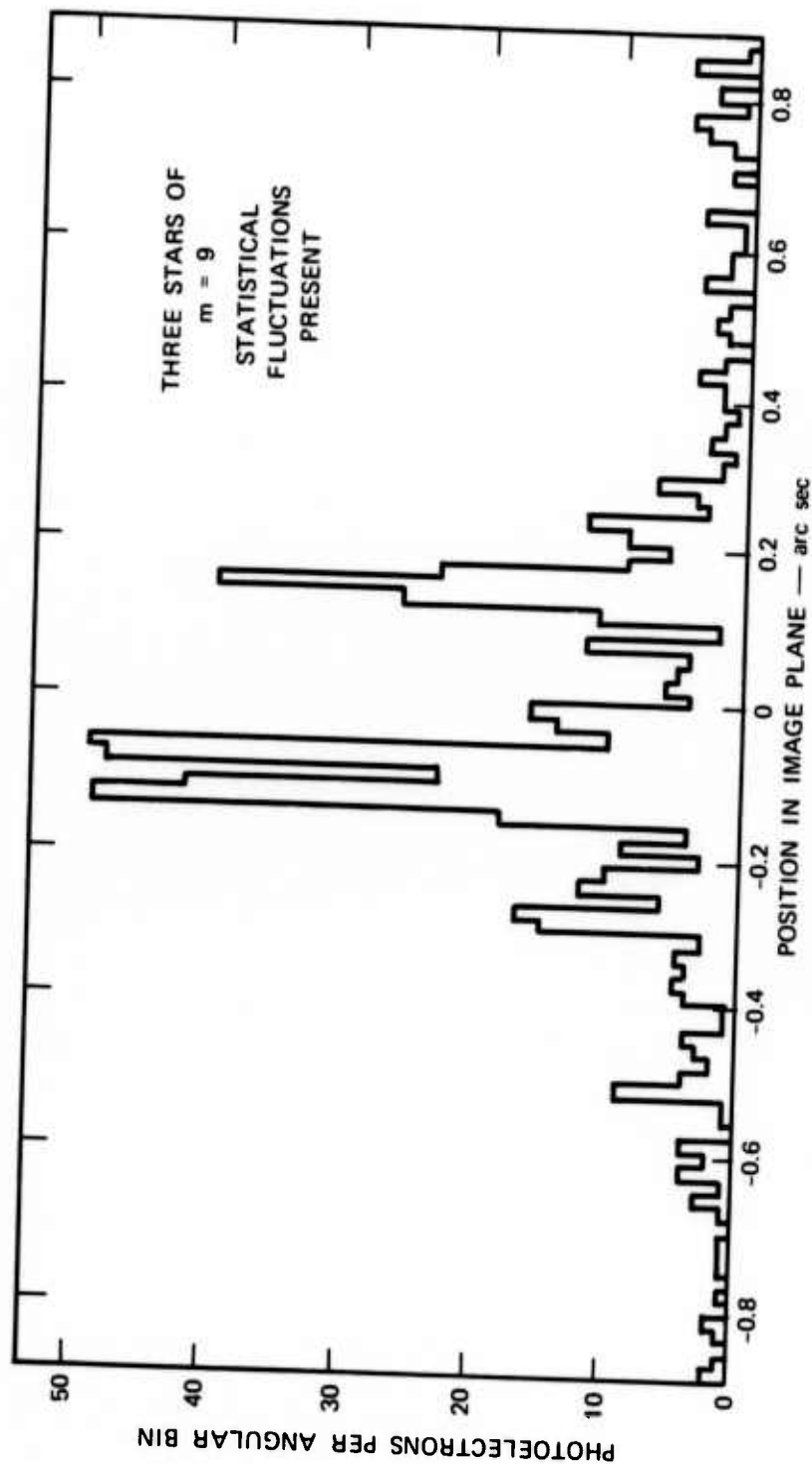
27

FIGURE 8   IMAGE OF A TRIPLE STAR, WITH PHOTOELECTRON STATISTICS CONSIDERED. The distorted wavefront was the same as that used in Figure 5, but a random-number generator varied the number of photoelectrons in each image bin according to Piosson statistics. Roughly 1000 photoelectrons were available for each measurement of the sharpness function S_1. For the strip mirror simulated here (25 elements of 100 cm2 each, photon detection efficiency $\eta = 0.25$, and time available for the correction $\tau = 0.02$ sec), each star would be 9th magnitude. Statistical fluctuations evident in the figure result from the very short effective exposure time used ($0.4 \times 10\text{-}3$ sec); a better image would result from the superposition of many such fast images at an observatory.

28

a strip mirror of 25 segments (each 100 cm^2), a quantum efficiency $\eta = 0.25$, and an atmospheric coherence time $\tau = 0.02$ sec. The average number of photoelectrons available for each calculation of S was 1000. When the number of photoelectrons was reduced by a factor of three, the image was severely degraded.

We define the image quality Q to be S/S_0, where S is the sharpness value achieved in the presence of statistical fluctuations, and S_0 is the value achieved if the statistical fluctuations were absent. A plot of Q versus number of photoelectrons is shown in Figure 9 for our simulations of an annular telescope consisting of 25 segments. Again, roughly 1000 photoelectrons per segment setting are needed in order to make a significant improvement in the image sharpness. Equation (7) would have predicted that $N^2 = 25^2 = 625$ photoelectrons are required.
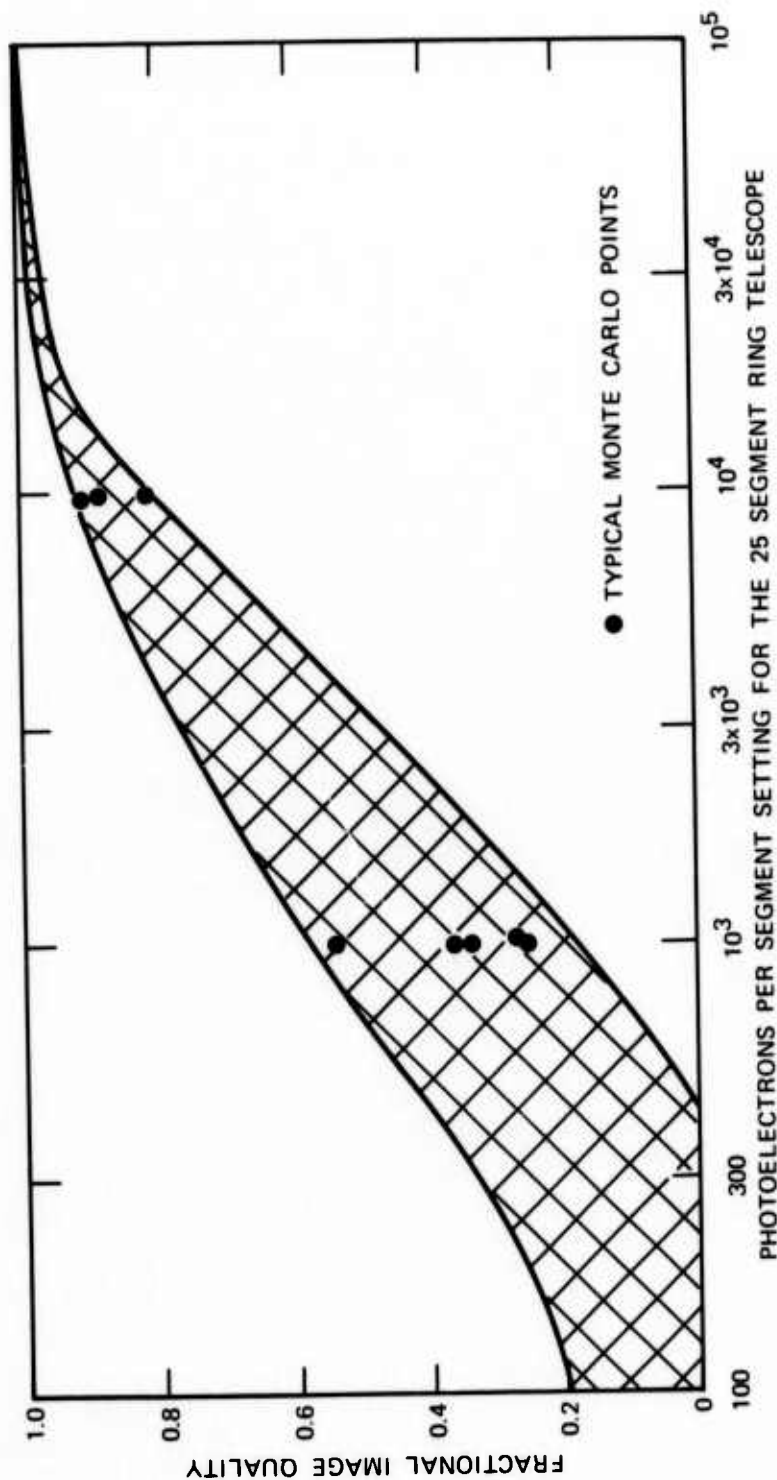
FIGURE 9   FRACTIONAL IMAGE QUALITY AFTER ONE ITERATION vs. NUMBER OF PHOTOELECTRONS PER SEGMENT SETTING.   Image quality $Q = S/S_0$, where S is the image sharpness after one iteration, and S_0 is the image sharpness for the simulation where no statistical fluctuations were applied.   The telescope geometry for this figure was the 0.75-m-diameter annular mirror with area $A = 2500$ cm^2. The hatched region indicates the typical range of variations in Q due to photoelectron fluctuations.   The sharpness function used was $S_3 = \int MI$, where $M = $ a round hole the same size as the central diffraction pattern of a point star.   The number of photoelectrons was defined to be 0.25 times the number of photons incident on the entire telescope in one setting time t.   Very similar results were found for S_1 and for the strip telescope geometry.

30

V   DISCUSSION AND CONCLUSIONS

We have shown in the preceding sections that a basically simple system of active telescope optics, using a sharpness-measuring device at the telescope image plane to feed back to a flexible optical element, should eliminate most of the image degradation caused by atmospheric distortion. A great variety of image-sharpness definitions can in principle drive the feedback system. The bandwidth of the flexible optical element, set by the characteristic time τ in which the atmospheric disturbance changes, appears to be within present-day technical reach. The angular size of an object that can be corrected this way is limited by the size of the isoplanatic patch. The angular extent of this patch depends not only on the physical size of the disturbed region, but also on its nearness to the telescope. For ground-based telescopes, the size of the patch is only a few seconds of arc,[12,13] whereas for airborne telescopes, where the turbulent layer is very close to the telescope, the size of the patch should extend out to many minutes of arc. This would be suitable for imaging large objects such as Jupiter.

The time τ also determines the minimum brightness of an object that can be corrected by this technique. Equation (6) relates the object flux B and τ to the particular parameters of the telescope system:

$$ B \geqslant \frac{n\,A^2}{a^3\,\tau\eta} \quad , $$

where

B = Object flux in photons/cm^2 sec at telescope

n = Number of segment settings needed to determine optimum position for that segment

A = Area (cm^2) of telescope aperture

a = Area (cm^2) of each adjustable segment

η = Quantum efficiency of detector

τ = Coherence time of the atmospheric distortion.

For ground-based telescopes, a is typically 100 cm^2 and $\tau \approx 0.02$ sec. Using Eq. (8) to relate B to stellar magnitude and choosing an annular telescope geometry to give the best resolution for a given A (the Rayleigh criterion for an annular ring gives $\theta = 0.76\lambda/D$), we can derive the following relationship between object magnitude and the best resolution obtainable assuming telescope parameters matched to the object:

$$\theta = \frac{10^{-3} \; \lambda \; 10^{m/5}}{a \; \sqrt{n\tau/n}}$$

where

θ = Best resolution (radians), Rayleigh criterion

λ = Wavelength of light, cm

m = Magnitude of object under observation.

As an example, take $m = 7$, $\lambda = 5 \times 10^{-5}$ cm, $\eta = 0.25$, $\tau = 0.02$ sec, $a = 100$ cm^2, and $n = 2$ settings. These yield a θ of 3×10^{-7} rad ≈ 0.06 arc sec. This resolution would be achieved with an annular telescope with a diameter of ≈ 130 cm ≈ 50 inches. Of course, one cannot usually match telescope parameters to particular objects. We present the calculation above only as a rough estimate of the resolution obtainable for a given magnitude with our system. A superior system, with a dimmer limiting magnitude for a given resolution, could be built by employing multiple-image systems, each with its own sharpness-measuring feedback scheme.[*]

---

[*] Multiple-image systems have been suggested to us by Jack Franck and Freeman Dyson.[22]

Note that the m that appears in our equations is the magnitude of the entire object (assuming it is all within an isoplanatic patch), not the magnitude of the feature under observation. Thus, for example, the light from a bright star can be used for image sharpening, even if the object under study is a dim companion.

A number of difficulties may arise if polychromatic light is used. First, the sharpness theorems were proven in the appendix just for monochromatic light. If the object is multicolored it is possible to increase $S_1 = \int I^2$ with a suitable aperture-plane distortion.[23] However, it can be shown[23] that the theorem for S_1 is still correct for polychromatic light as long as the object is uniformly colored--i.e., each point on the object emits light with the same spectrum. Second, the lateral color aberration produced by the atmosphere will disperse the image unless one is viewing close to the zenith. Hill and Zanoni[24] have proposed a telescope modification that adequately corrects for this. Third, there is the possibility that an aperture segment in our system reaches a setting different from the true setting by 2π radians. Figure 6 shows two segments for which this happened. For monochromatic light such a shift makes no difference, but for polychromatic light it causes some image degradation. Of course a narrow-bandpass filter would solve these problems, but at a cost in least correctable magnitude. For the third problem, we expect that the telescope feedback system will "lock in" on the correct phase-distortion distributions as they drift across the aperture of the telescope. In any case, if one wanted, the telescope could have a "search mode" in which 2π phase shifts are also tried on the individual movable segments to see if any improvement lies in that direction.

The image-sharpening technique discussed here can be used for more than just the elimination of atmospheric distortion. Since maximizing of S automatically refigures in the telescope optics, sharpening could

33

be used to refigure lightweight optics either on the ground or in space. Image sharpening can also be applied to radio-interferometric measurements where, for long-baseline multielement systems, the relative phases of the receivers are unknown. These phases can be determined in the computer analysis by calculating the values that maximize the sharpness of the radio image.

Our research group at Berkeley is currently designing a compensating system that could be attached near the focal plane of existing optical telescopes.

Appendix

PROOFS THAT SHARPNESS FUNCTIONS REACH MAXIMA
FOR THE RESTORED IMAGE

Appendix

PROOFS THAT SHARPNESS FUNCTIONS REACH MAXIMA
FOR THE RESTORED IMAGE

Consider an image plane (x,y) where we observe an intensity distribution $I(x,y)$ of focused light from a distant object of small angular extent. The focusing is provided by a telescope objective placed a distance f away. Let (u,v) be the coordinates at the aperture (objective) plane, and consider the objective and the image planes both to be perpendicular to the line connecting the center of the objective and the center of the light distribution of the distant object. The intensity $I(x,y)$ is then given by a modified Fresnel-Kirchoff integral over the surface of the telescope objective:

$$I(x,y) = \int d\theta \ d\phi \ O(\theta,\phi) \ \left| \int du \ dv \ e^{ik[\delta(u,v)+(ux+vy)/f+(u\theta+v\phi)]} \right|^2$$

$$(A-1)$$

where we have neglected the angular obliquity factors.[25] Here k is the wavenumber of the light (which we take to be monochromatic), $O(\theta,\phi)$ is the light flux from angles (θ,ϕ) falling on the telescope objective, and we have assumed that the object under observation is radiating incoherently. The real function $\delta(u,v)$ includes both the effects of the disturbing atmosphere and of the correcting optical elements. As we have stated in the main text, we have ignored the fact that the atmosphere modulates the amplitude as well as the phase of the incoming wave. The assumption that the entire object falls within an isoplanatic patch is equivalent to the assumption that the atmospheric distortion can be written in the form $\delta(u,v)$ instead of the more general form $\delta(u,v,\theta,\phi)$.

36

1.   Proof that Sharpness Functions S_1 and S_4 Reach Absolute
     Maxima for a Restored Image

S_1 is a special case of the more general sharpness function S_4,
defined in Table 1 of the main text:

$$S_4 = \int dx\ dy\ \left| \frac{d^{\ell+m} I(x,y)}{dx^{\ell}\ dy^{m}} \right|^2 \quad . \tag{A-2}$$

For convenience, we rewrite Eq. (A-1) eliminating the square by intro-
ducing the dummy variables u' and v':

$$I(x,y) = \int d\theta\ d\phi\ 0(\theta,\phi)\ \int du\ du'\ dv\ dv'$$

$$\cdot\ e^{ik[\delta(u,v)-\delta(u',v')+(u-u')x/f+(v-v')y/f]}$$

$$\cdot\ e^{ik[(u-u')\theta+(v-v')\phi]} \quad . \tag{A-3}$$

We now substitute Eq. (A-3) into Eq. (A-2), perform the differentiation,
and write out the square by introducing new dummy variables:

$$S_4 = \int dx\ dy \int d\theta_1\ d\theta_2\ d\phi_1\ d\phi_2\ 0(\theta_1,\phi_1)\ 0(\theta_2,\phi_2)\ du_1\ du'_1\ du_2\ du'_2\ dv_1\ dv'_1\ dv_2\ dv'_2$$

$$\cdot\ (k/f)^{2(\ell+m)}\ (u_1-u'_1)^{\ell}\ (v_1-v'_1)^{m}\ (u_2-u'_2)^{\ell}\ (v_2-v'_2)^{m}$$

$$\cdot\ e^{ik[(u_1-u'_1)(x/f+\theta_1)+(v_1-v'_1)(y/f+\phi_1)]}$$

$$\cdot\ e^{ik[(u_2-u'_2)(x/f+\theta_2)+(v_2-v'_2)(y/f+\theta_2)]}$$

$$\cdot\ e^{ik\{\delta(u_1,v_1)-\delta(u'_1,v'_1)+\delta(u_2,v_2)-\delta(u'_2,v'_2)\}} \quad . \tag{A-4}$$

The integral over x and y can now be performed, yielding Dirac delta-
functions: $\delta_D(u_1-u'_1+u_2+u'_2)$ and $\delta_D(v_1-v'_1+v_2-v'_2)$.   The integral over

37

these delta-functions can be performed immediately, eliminating one each
of the u and v variables. Defining new variables $z = u_1 - u_1'$ and
$w = v_1 - v_1'$, we obtain

$$
S_4 = (2\pi)^2 \int d\theta_1 \ d\theta_2 \ d\phi_1 \ d\phi_2 \ 0(\theta_1,\phi_1) 0(\theta_2,\phi_2) \int du_1 \ dz \ du_2 \ dv_1 \ dw \ dv_2
$$

$$
\cdot \ (k/f)^{2(\ell+m-1)} \ z^{2\ell} \ w^{2m} \ e^{ik[(\theta_1-\theta_2)z+(\phi_1-\phi_2)w]}
$$

$$
\cdot \ e^{ik\{\delta(u_1,v_1)-\delta(u_1-z,v_1-w)+\delta(u_2,v_2)-\delta(u_2+z,v_2+w)\}} \tag{A-5}
$$

Since the term in the brackets $\{\}$ does not involve the θ's or the ϕ's,
we can perform the integrals over these variables, which result in
Fourier transforms of the original intensity distributions. Let the
Fourier transform of $0(\theta,\phi)$ be $\widetilde{0}$ (kz,kw). Then we can rewrite Eq. (A-5):

$$
S_4 = (2\pi)^3 \int du_1 \ dz \ du_2 \ dv_1 \ dw \ dv_2 \ (k/f)^{2(\ell+m-1)} \ z^{2\ell} \ w^{2m} \ \left| \widetilde{0}(kz,kw) \right|^2 e^{ik\{\ldots\}} ,
$$

$$
\tag{A-6}
$$

where the term in brackets $\{\ldots\}$ is the same as in the preceding equation.
Except for the exponential, the integrand in Eq. (A-6) is positive-
definite. Therefore the integral will reach its maximum value when the
exponential is identically equal to one--i.e., the term in brackets
$\{\ldots\}$ = 0. This term is identically zero only if $\delta(u,v)$ is zero, or
at most a linear function of u and v:

$$
\delta(u,v) = a + bu + cv \tag{A-7}
$$

where a, b, and c are constants. A linear variation of $\delta(u,v)$ results
in a shift in the image position, but in no image distortion. Therefore
we have proven that maximizing S_4 restores all but the original position
of the undistorted image.

2. Proof that S_5 Reaches an Absolute Maximum for an Unresolved Star

In Table 1 of the main text we defined S_5:

$$S_5 = \int dx\ dy\ I^n(x,y) \qquad n \geqq 2\ ,\quad \text{integer} \qquad . \qquad (A-8)$$

For an unresolved star, $O(\theta,\varphi)$ is a Dirac delta function, which for convenience we put at $\theta = 0$ and $\varphi = 0$. Then, going through a derivation similar to that given for S_4, we can rewrite Eq. (A-8):

$$S_5 = \left(\frac{2\pi f}{k}\right)^2 O^n(0,0)\ \int d^n u\ d^n v\ d^{n-1} z\ d^{n-1} w\ e^{ik\{\ldots\}} \qquad , \qquad (A-9)$$

where the brackets $\{\ldots\} =$

$$\sum_{j=1}^{n-1} [\delta(u_j,v_j) - \delta(u_j - z_j, v_j - w_j)] + \delta(u_n,v_n) - \delta\left(u_n + \sum_{j=1}^{n-1} z_j, v_n + \sum_{j=1}^{n-1} w_j\right)$$

and contain the effect of the atmospheric perturbation. As in the preceding proof, S_5 will have its absolute maximum only when $\{\ldots\} = 0$, which again implies that $\delta(u,v)$ is at most a linear function of its arguments--i.e., when the atmospheric distortion has been removed.

3. Maximum Theorem for S_3 and S_8 (Image-Defect Functions)

S_3 and S_8 are examples of sharpness definitions in which the observed intensity $I(x,y)$ is compared with a standard of reference. If we have advance knowledge of the undistorted intensity distribution $I_0(x,y)$, then we can attempt to maximize the image-defect function S_8:

$$S_8 = -\int dx\ dy\ \left| I(x,y) - I_0(x,y) \right|^2 \qquad . \qquad (A-10)$$

39

This function obviously reaches its maximum value (zero) only when $I(x,y)$ exactly matches $I_0(x,y)$. If we expand the square we get

$$S_8 = - \int dx\; dy\; I^2(x,y) + 2 \int dx\; dy\; I_0(x,y)\; I(x,y) - \int dx\; dy\; I_0^2(x,y) \quad .$$

(A-11)

The first term in this equation is $-S_1$; the second term is $2S_3$ for the particular case when $M(x,y) = I_0(x,y)$; and the third term is a constant. Since S_8 is maximized at the restored image and the S_1 is also maximized, it follows that S_3 must also reach its absolute maximum if Eq. (A-10) is to be correct.

We have not made analytic studies of what happens if the function $M(x,y)$ in S_3 does not match $I_0(x,y)$, except in the case where M is a Dirac delta function, in which case S_3 reduces to S_2, and in the case where $M(x,y) = -x^2 - y^2$ (for which S_3 is equal to S_6 of Table 1), where a maximum proof has been obtained.[24] Our computer simulations indicate that $M(x,y)$ can depart from $I_0(x,y)$ in substantial ways before our iteration technique fails to converge on a true image. All the defect functions have the feature that they automatically center the image as well as sharpen it.

ACKNOWLEDGMENTS

REFERENCES

1. Sir Isaac Newton, Optics, Book 1, Part I, Prop VIII, Prob II. (1730), (Dover Publications, Inc., New York, N.Y., 1952).

2. D. Kelsall, J. Opt. Soc. Am., Vol. 63, p. 1472 (1973).

3. R. E. Danielson, "High Resolution Imagery with the Large Space Telescope," in Astronomy from a Space Platform, Vol. 28, pp. 197-212, Science and Technology series, (American Astronautical Society, Tarzana, Calif., 1972.)

4. A. A. Michelson and F. G. Pease, Astrophys. J., Vol. 53, p. 249 (1921).

5. R. H. Brown and R. Q. Twiss, Nature, Vol. 178, p. 1046 (1956); Proc. Roy. Soc., Vol. A 248, 199, 222 (1958).

6. A. Labeyrie, Astronomy and Astrophys., Vol. 6, p. 85 (1970); D. Gezari, A. Labeyrie, and R. Stacknik, Astrophys. J., Vol. 173, No. L1 (1972).

7. W. T. Rhodes and J. W. Goodman, J. Opt. Soc. Am., Vol. 63, p. 647 (1973).

8. "Restoration of Atmospherically Degraded Images," Woods Hole Summer Study (National Academy of Science, Washington, D.C., 1966).

9. A. D. Code, "New Generation Optical Telescope Systems," Ann. Rev. Astron. Astrophys., Vol. 11, pp. 239-268 (1973).

10. W. A. Baum, D. M. Busby, and T. V. Pettauer, "The Stabilization of Planetary Images," "Photo-Electronic Image Devices," pp. 781-788, Vol. 33B, Advances in Electronics and Electron Physics, Academic Press Inc., New York, N.Y.,(1972); R. B. Leighton, Sci. Am., Vol. 6, p. 156 (1956).

11. H. W. Babcock, Publ. Astron. Soc. Pac., Vol. 65, p. 229 (1953); H. W. Babcock, J. Opt. Soc. Am., Vol. 48, p. 500 (1958).

12. I. G. Kolchinskii, "Correlation Between Image Pulsations of Stars at a Small Angular Distance from Each Other," in *Optical Instability of the Earth's Atmosphere*, N. I. Kucherov, ed., pp. 7-19 (Moscow, 1965).

13. P. A. Button, M. F. Reusch, B. Sage and D. Duke, "Measurements of the Extent of the Atmospheric Spatial Isoplanatic Region," ARPA Order Number 763, Contract FO 8606-68-C-0045; also an abstract appears for talk TuH16, 1970 annual meeting of the Optical Society of America, *J. Opt. Soc. Am.*, Vol. 60, p. 1550 (1970).

14. R. E. Hufnagel and N. R. Stanley, *J. Opt. Soc. Am.*, Vol. 54, p. 52 (1964); R. E. Hufnagel, Appendix 3, Vol. 2 of Ref. 8.

15. D. L. Fried, *J. Opt. Soc. Am.*, Vol. 56, p. 1372 (1966); Also, D. L. Fried, *Proc. IEEE*, Vol. 55, No. 1 (January 1967).

16. J. L. Bufton, P. O. Minott, and M. W. Fitzmaurice, *J. Opt. Soc. Am.*, Vol. 62, p. 1068 (1972); also, A. Labeyrie, private communication.

17. H. F. Wischnia, "Active Optics for Space Astronomy," in *Astronomy from a Space Platform*, Vol. 28, pp. 347-361, Science and Technology Series (American Astronautical Society, Tarzana, Calif., 1972).

18. F. J. Dyson, *Theory of Optical Image Improvement* (to be published).

19. E. H. Linfoot, *J. Opt. Soc. Am.*, Vol. 46, p. 740 (1956).

20. See, for example, "Technology Trends," *Optical Spectra*, p. 46 (October 1973).

21. C. W. Allen, *Astrophysical Quantities*, 2nd Ed., p. 191 (Oxford Press, New York, N.Y., 1964).

22. J. Franck and F. Dyson, private communications.

23. F. J. Dyson, private communication.

24. H. A. Hill and C. A. Zanoni, *J. Opt. Soc. Am.*, Vol. 56, p. 1655 (1966).

25. M. Born and E. Wolf, *Principles of Optics*, 3rd Ed., p. 380 (Pergamon Press, New York, N.Y., 1965).